SUPPLEMENTARY INFORMATION

Nearly Perfect Spin Polarization of Noncollinear Antiferromagnets

Gautam Gurung[1,2,3*], Mohamed Elekhtiar[1], Ding-Fu Shao[4,†], and Evgeny Y. Tsymbal[1,‡]

[1] *Department of Physics and Astronomy & Nebraska Center for Materials and Nanoscience, University of Nebraska, Lincoln, Nebraska 68588-0299, USA*

[2] *Clarendon Laboratory, Department of Physics, University of Oxford, Parks Road, Oxford, OX1 3PU UK*

[3] *Trinity College, University of Oxford, Oxford OX1 3BH, UK*

[4] *Key Laboratory of Materials Physics, Institute of Solid-State Physics, HFIPS, Chinese Academy of Sciences, Hefei 230031, China*

A. Band structure and spin polarization of a magnetic Kagome lattice

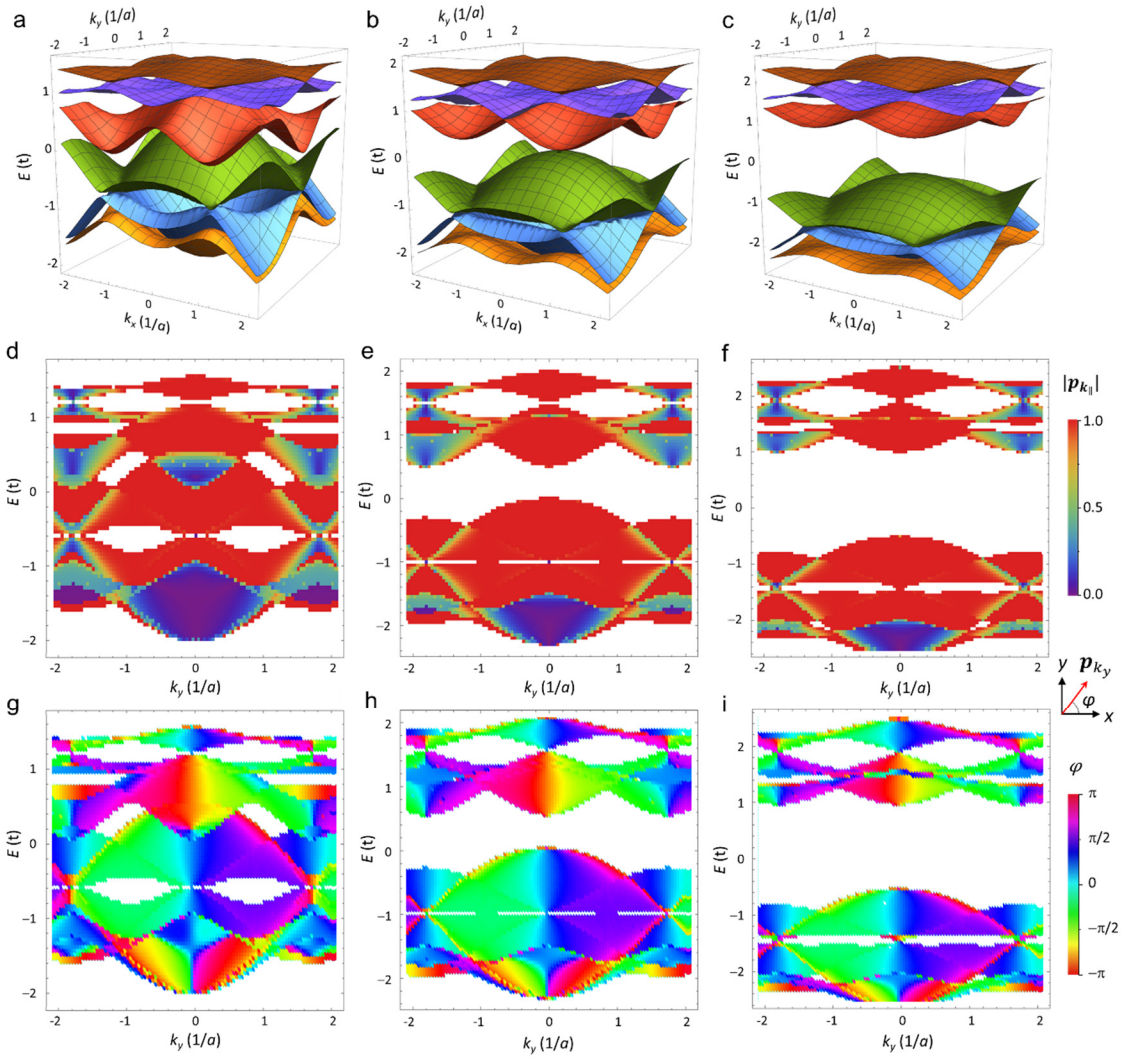

Fig. S1: Band structure (**a**-**c**) and spin polarization vector $\boldsymbol{p}_{k_y}$ as a function of k_y and energy E (**d**-**i**) for non-collinear magnetic Kagome lattice (shown in Fig. 1a) for $\Delta/t = 1$ (**a**, **d**, **g**), $\Delta/t = 2$ (**b**, **e**, **h**), and $\Delta/t = 3$ (**c**, **f**, **i**). $\boldsymbol{p}_{k_y}$ vectors lie in the *x*-*y* plane ($p_z = 0$). Their magnitudes $p_k \equiv |\boldsymbol{p}_k|$ (**d**-**f**) and polar angles φ (**g**-**i**) are depicted in color.

B. Spin textured Fermi surface of $GaNMn_3$

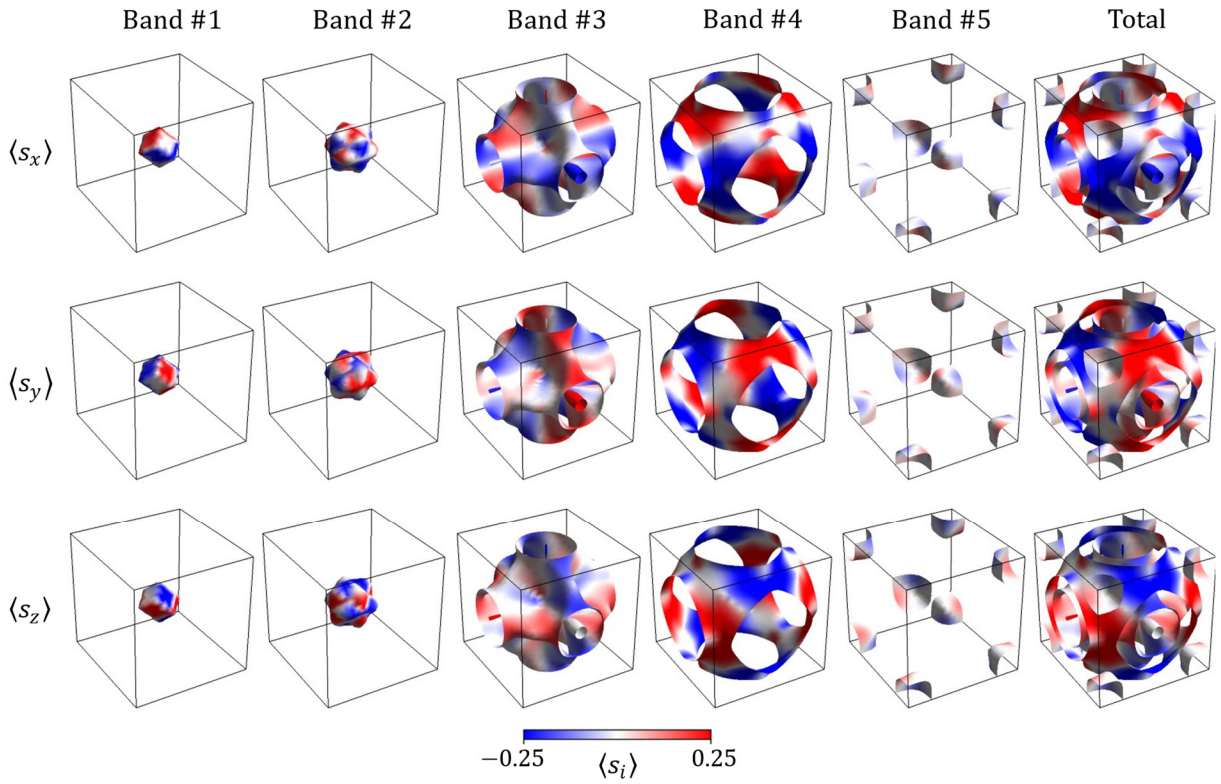

Fig. S2: Spin-textured Fermi surface of $GaNMn_3$ in the Γ_{5g} phase. The expectation values of spin components are shown in color.

C. Spin-resolved band structure of $GaNMn_3$

Figure S3 shows the spin-resolved band structure of $GaNMn_3$ in the Γ_{5g} phase (Fig. S3 (a)) and Fermi surface bands crossing different k_z-planes (Fig. S3 (b)). Sizable spin expectation values (and thus spin polarization) result from a large spin splitting of the band structure. It is seen from Fig. S3 (b) that along the $k_x = 0$ and $k_y = 0$ lines and in adjacent areas, the $\langle s_x \rangle$, $\langle s_y \rangle$, and $\langle s_z \rangle$ spin components have the same signs for a given $\boldsymbol{k}_{\parallel}$. This leads to the cross-pattern feature in the distributions of spin and spin polarization in the 2DBZ that are shown in Fig. 3 in the main text.

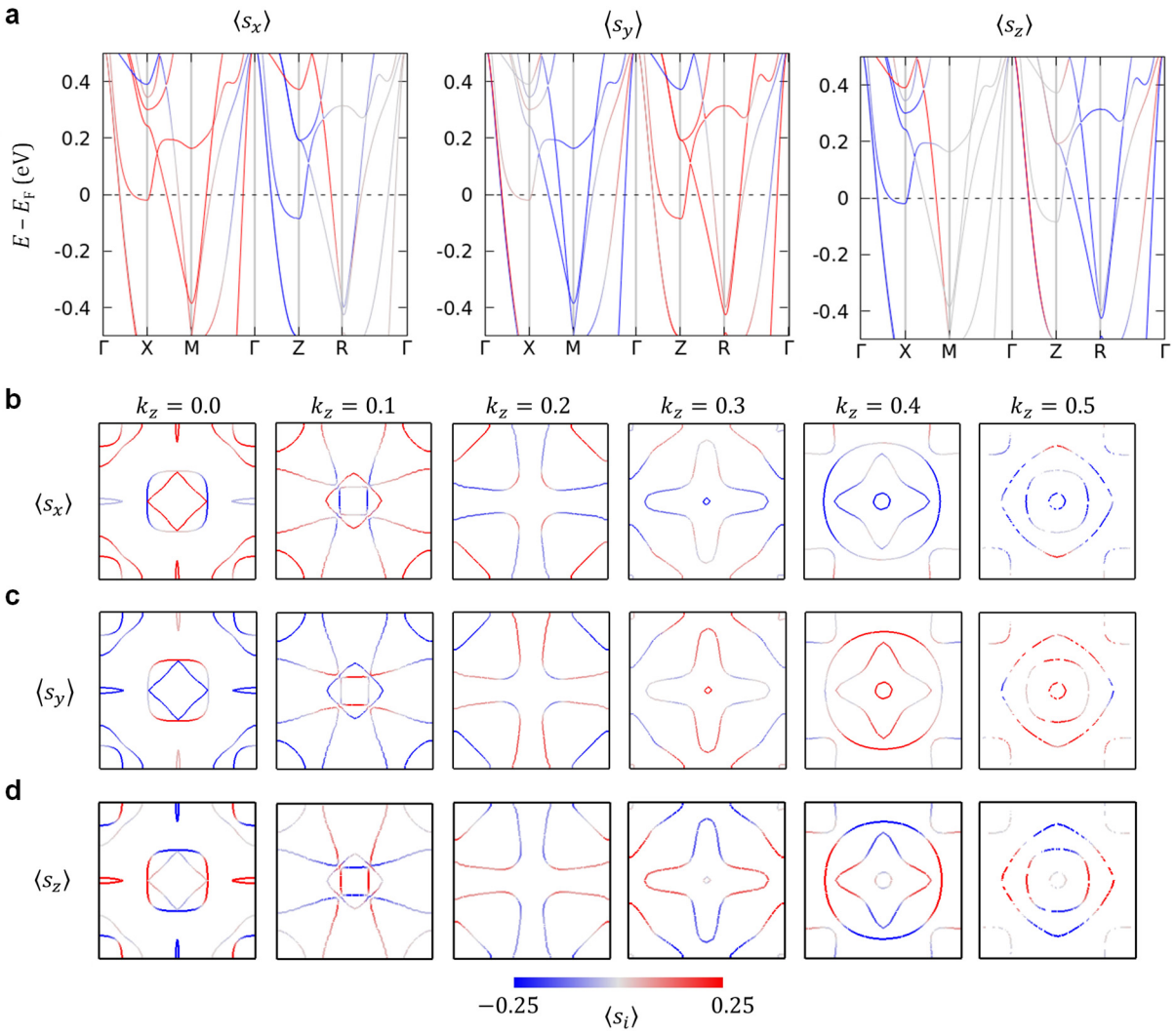

Fig. S3: Spin-resolved band structure of $GaNMn_3$ in the Γ_{5g} phase. (**a**) Band structure with projected spin polarization components $\langle s_i \rangle, i = x, y, z$. Fermi surface cuts at $k_z = 0.0, 0.1, 0.2, 0.3, 0.4, 0.5$ planes with projected spin components: (**b**) $\langle s_x \rangle$, (c) $\langle s_y \rangle$, (**c**) $\langle s_z \rangle$, respectively. Color indicates the strength of the spin polarization component.

D. Persistent spin texture

We observe that some regions in the 2DBZ of Mn_3GaN (001) exhibit a persistent spin texture, where spins are pointing in the same direction. Figure S4 shows color mapped azimuthal θ and polar φ angles of the spin polarization vector of Mn_3GaN in the (001) 2DBZ. It is seen that in the areas indicated by dashed lines both θ and φ angles remain nearly constant indicating the same orientation of the polarization vector. This is the signature of the persistent spin texture.

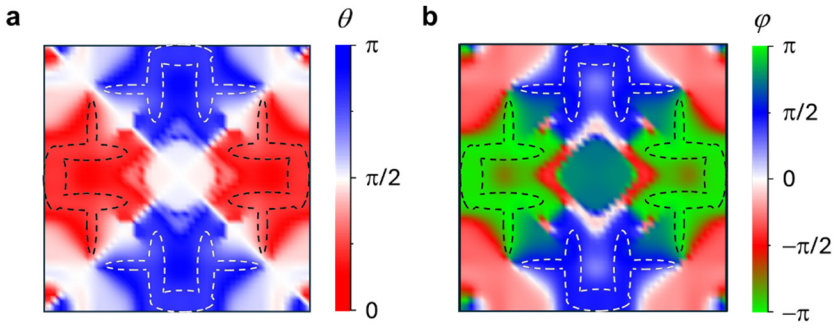

Fig. S4: Azimuthal θ (**a**) and polar φ (**b**) angles of the spin polarization vector of Mn_3GaN color mapped in the (001) 2D Brillouin zone. Dashed lines (both black and white) indicate areas with persistent spin texture.

E. Layer-resolved spectral density of $Mn_3GaN/SrTiO_3/Mn_3GaN$ AFMTJ

Here we calculate the layer-resolved spectral density (i.e. layer- and $\boldsymbol{k}_\parallel$-resolved density of states) projected onto the $s_z = \pm ½$ spin states, $D^{s_z}(\boldsymbol{k}_\parallel)$, for an $Mn_3GaN/SrTiO_3/Mn_3GaN$ AFMTJ. Figure S5(a) shows the results for the interfacial and bulk-like components of $D^{s_z}(\boldsymbol{k}_\parallel)$ for Mn_3GaN electrodes. It is seen that the $s_z = +½$ and $s_z = -½$ projections of the spectral density are related by the mirror symmetry $\widehat{M}_{110}$ (or $\widehat{M}_{\bar{1}10}$) transformation similar to the $s^z_{\boldsymbol{k}_\parallel}$ spin component shown in Fig. 3c of the main text. Importantly, the interfacial and bulk-like $D^{s_z}(\boldsymbol{k}_\parallel)$ of Mn_3GaN exhibit similar distribution in the 2DBZ, indicating that the spin-dependent features of the band structure of Mn_3GaN do not change much when moving from the bulk to the interface.

This behavior is also seen from the spin polarization of the spectral density, which is defined as $P^z(\boldsymbol{k}_\parallel) = \frac{D^{½}(\boldsymbol{k}_\parallel) - D^{-½}(\boldsymbol{k}_\parallel)}{D^{½}(\boldsymbol{k}_\parallel) + D^{-½}(\boldsymbol{k}_\parallel)}$. As is evident from Fig. S5(c), $P^z(\boldsymbol{k}_\parallel)$ is antisymmetric with respect to diagonals $[110]$ and $[\bar{1}10]$ of the 2DBZ and zero at the diagonals. These features are analogous to those revealed by the z-component of the momentum-dependent spin polarization $p^z_{\boldsymbol{k}_\parallel}$ in Fig. 3e of the main text. Importantly, the interfacial and bulk-like spin polarizations of the spectral density exhibit similar patterns in the 2DBZ, indicating that the non-vanishing spin polarization in the $Mn_3GaN/SrTiO_3/Mn_3GaN$ AFMTJ is preserved at the interface.

Looking at the interfacial and bulk-like components of $D^{s_z}(\boldsymbol{k}_\parallel)$ in the $SrTiO_3$ barrier layer (Fig. S5(b)), we observe a pronounced cross pattern reflecting the features of the evanescent states in bulk $SrTiO_3$ shown in Fig. 4b of the main text. Again, we see that the interfacial and bulk-like components of $D^{s_z}(\boldsymbol{k}_\parallel)$ are similar, demonstrating that the interface does not destroy the properties of the evanescent states obtained from the complex band structure of bulk $SrTiO_3$.

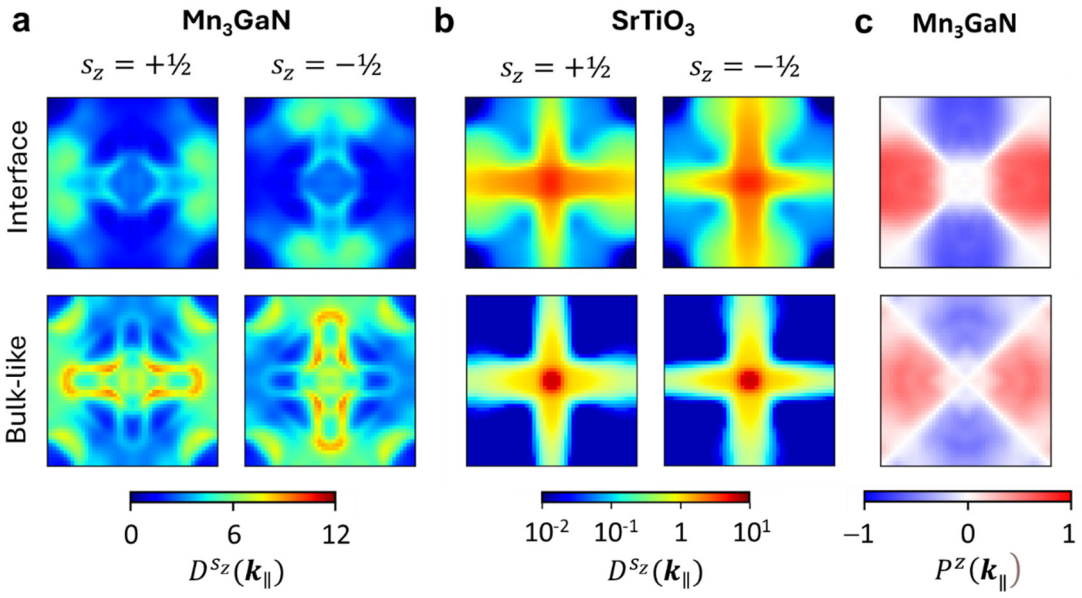

Fig. S5: (a,b) Layer-resolved spectral density $D^{s_z}(\boldsymbol{k}_\parallel)$ projected onto the $s_z = \pm ½$ spin states for an $Mn_3GaN/SrTiO_3/Mn_3GaN$ AFMTJ: interfacial (top panels) and bulk-like (bottom panels) components of $D^{s_z}(\boldsymbol{k}_\parallel)$ for Mn_3GaN (**a**) and $SrTiO_3$ (**b**). The interfacial and bulk-like components of the spectral density are calculated by projecting $D^{s_z}(\boldsymbol{k}_\parallel)$ to the interfacial unit cell and middle unit cell of the Mn_3GaN or $SrTiO_3$ slabs, respectively. (**c**) Spin polarization of spectral density $P^z(\boldsymbol{k}_\parallel)$ for interfacial (top) and bulk-like (bottom) Mn_3GaN.

F. Energy dependent spin polarization of Mn_3GaN

Figure S6 shows the calculated components of the effective spin polarization $\boldsymbol{p}_{k_\parallel} = (p^x_{\boldsymbol{k}_\parallel}, p^y_{\boldsymbol{k}_\parallel}, p^z_{\boldsymbol{k}_\parallel})$ and polarization magnitude $p_{\boldsymbol{k}_\parallel} \equiv |\boldsymbol{p}_{\boldsymbol{k}_\parallel}|$ of Mn_3GaN for different energies E. It is seen that at $E = E_F - 0.25$ eV the cross pattern of nearly perfect spin polarization is sustained and even becomes more apparent, while at $E = E_F - 0.5$ eV it becomes less pronounced, resulting in some reduction of the ETMR value at this energy (Fig. 4g in the main text).

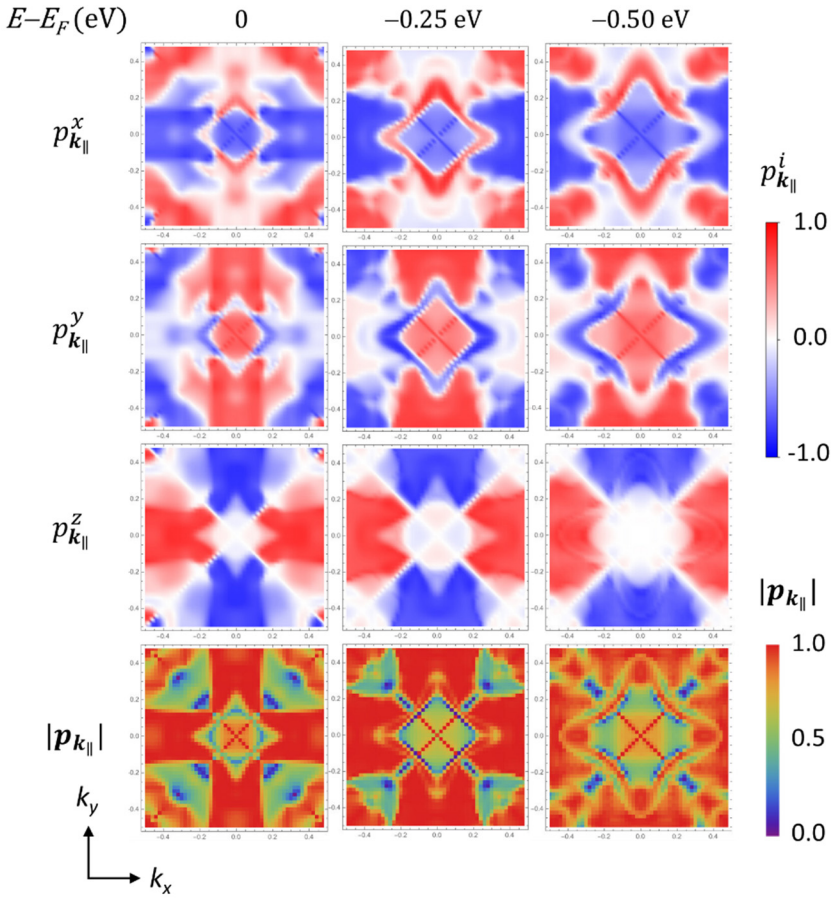

Fig. S6: Components of the effective spin polarization $\boldsymbol{p}_{k_\parallel} = (p^x_{\boldsymbol{k}_\parallel}, p^y_{\boldsymbol{k}_\parallel}, p^z_{\boldsymbol{k}_\parallel})$ (three top panels in each column) and polarization magnitude $p_{\boldsymbol{k}_\parallel} \equiv |\boldsymbol{p}_{\boldsymbol{k}_\parallel}|$ (bottom panels) of bulk Mn_3GaN (001) for different energies E indicated on top.

G. Complex band structure of $SrTiO_3$

Figure S7 shows the calculated complex band structure of $SrTiO_3$. It is seen that the lowest decay rates of the evanescent states for different energies in the band gap of $SrTiO_3$ appear along the $k_x = 0$ and $k_y = 0$ lines, exhibiting a cross-pattern feature that matches the highly spin polarized states in $GaNMn_3$.

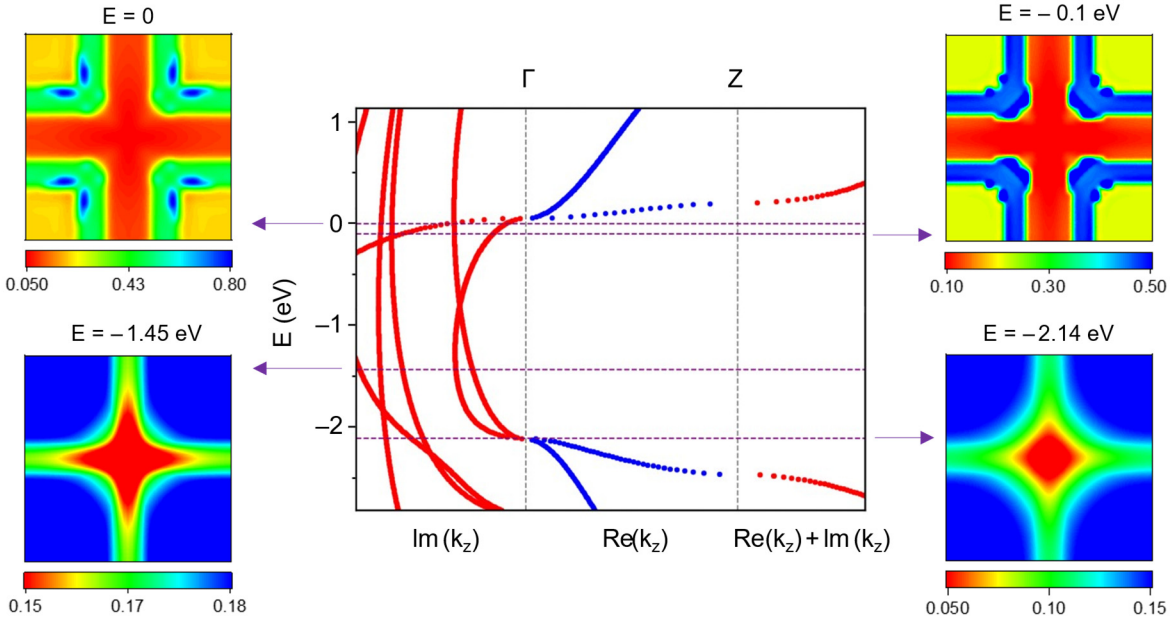

Fig. S7: The calculated complex band structure of $SrTiO_3$ linking real bands along the high-symmetry Γ-Z line and complex bands at the $\bar{\Gamma}$ and $\bar{Z}$ points. The insets show the lowest decay rate in the 2DBZ at different energies.

H. Effects of spin-orbit coupling

Here we explore the effects of spin-orbit coupling (SOC) on the spin polarization of bulk Mn_3GaN (001) and ETMR in $Mn_3GaN/SrTiO_3/Mn_3GaN$ (001) AFMTJs using fully relativistic PAW pseudopotentials in the DFT calculations. The results for the spin polarization of bulk Mn_3GaN (001) in the presence of SOC are shown in Figure R8a in comparison to Figure R8b which is obtained without including SOC in the calculation (the same as Fig. 3f in the revised manuscript). We see that the SOC effect on the spin polarization is insignificant and does not qualitatively change the overall picture. Importantly it preserves the cross-pattern feature of $p_{\boldsymbol{k}_\parallel}$ which is important for ETMR in $Mn_3GaN/SrTiO_3/Mn_3GaN$ (001) AFMTJs. Figures R8d,f show the results for the $\boldsymbol{k}_\parallel$-resolved transmission in $Mn_3GaN/SrTiO_3/Mn_3GaN$ (001) AFMTJs for parallel (Fig. R8d) and antiparallel (Fig. R8f) alignment of the Néel vector in the Mn_3GaN electrodes calculated in the presence of SOC. By comparing these results to those where SOC is neglected (Figs. R8d,f, the same as Figs. 4e,f in the revised manuscript), we see that they look very similar. There is though some enhancement of transmission due to SOC around the $\bar{\Gamma}$ point in the 2DBZ for the antiparallel alignment of the Néel vector (compare Figs. R8f and R8e), which leads to reduction of the ETMR ratio from 1.8×10^4% to 2.6×10^3%. Despite this reduction, the ETMR effect remains huge. We conclude therefore that SOC does not qualitatively change the main conclusions of our work. We note however that the SOC effects may be more pronounced in AFMTJs based on non-collinear antiferromagnets with heavy elements like Mn_3Ir and Mn_3Pt.

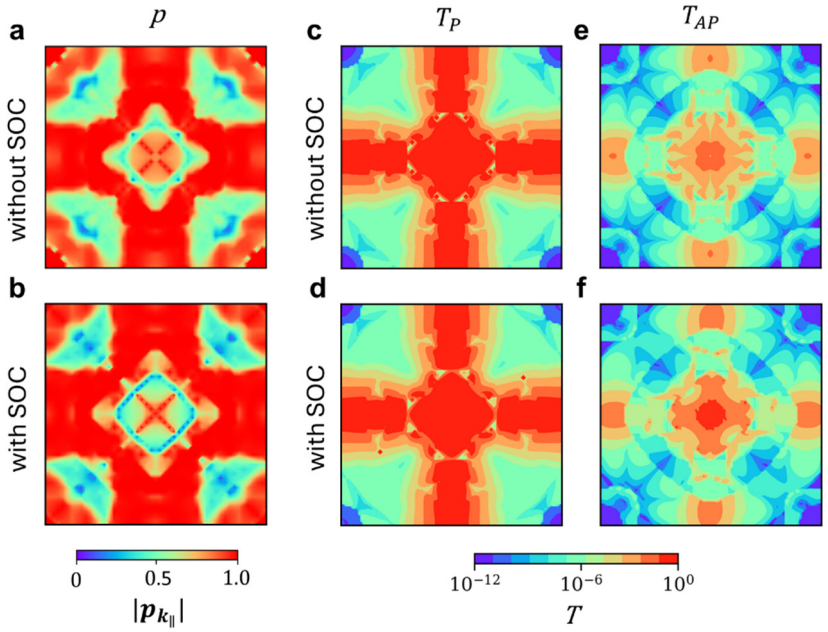

Fig. S8: Effects of SOC on the spin polarization of bulk Mn_3GaN (001) and ETMR in $Mn_3GaN/SrTiO_3/Mn_3GaN$ (001) AFMTJs. (**a**,**b**) $\boldsymbol{k}_\parallel$-resolved spin polarization of bulk Mn_3GaN (001) calculated without (**a**) and with (**b**) SOC. (**c**-**f**) $\boldsymbol{k}_\parallel$-resolved transmission in the 2DBZ for the AFMTJ for parallel (P) (**c**,**d**) and antiparallel (AP) (**e**,**f**) alignment of the Néel vector in the Mn_3GaN electrodes calculated without (**c**,**e**) and with (**d**,**f**) SOC.